ELSEVIER

Journal of Alloys and Compounds 444–445 (2007) 415–423

Journal of ALLOYS AND COMPOUNDS

www.elsevier.com/locate/jallcom

Models and simulations of nuclear fuel materials properties

M. Stan [a,*], J.C. Ramirez [a], P. Cristea [b], S.Y. Hu [a], C. Deo [a], B.P. Uberuaga [a], S. Srivilliputhur [a], S.P. Rudin [a], J.M. Wills [a]

[a] *Los Alamos National Laboratory, PO Box 1663, Los Alamos, NM 87545, USA*
[b] *University of Bucharest, Faculty of Physics, Bucuresti-Magurele, Romania*

Received 1 September 2006; received in revised form 17 January 2007; accepted 19 January 2007
Available online 24 January 2007

Abstract

To address the complexity of the phenomena that occur in a nuclear fuel element, a multi-scale method was developed. The method incorporates theory-based atomistic and continuum models into finite element simulations to predict heat transport phenomena. By relating micro and nano-scale models to the macroscopic equilibrium and non-equilibrium simulations, the predictive character of the method is improved. The multi-scale approach was applied to calculations of point defect concentration, helium bubbles formation, oxygen diffusivity, and simulations of heat and mass transport in UO_{2+x}.

Keywords: Actinide alloys and compounds; Nuclear reactor materials; Oxide materials; Microstructure; Point defects; Thermodynamic properties; Thermochemistry; Computer simulations; Molecular dynamics Simulations; Thermodynamic modeling

1. Introduction

Nuclear fuel materials (alloys and ceramics) are complex and often exposed to severe irradiation environments during manufacturing, operation, and storage. Most commercial fuel performance codes incorporate models of materials properties that are based on empirical correlations. The applicability of such models is limited to a regime where experimental data is available and extrapolation outside this regime may lead to misleading results.

An example of integration of various time and length scales is the prediction of the Pu–Ga phase diagram, in the low Ga content region [1]. Based on a method for determining phase stability in binary systems [2], the equilibrium phase diagram of Pu–Ga was calculated using limited information about the components. Electronic structure calculations provided input for the modified embedded atom method (MEAM). Molecular dynamics calculations using the MEAM many-body inter-atomic potential led to predictions of the free energy of all phases in the low temperature, low Ga content region of the Pu–Ga system [1]. The existence of a eutectoid point that involves monoclinic Pu, face centered cubic (fcc) Pu, and the Pu_3Ga compound was predicted confirming the metastable character of the fcc Pu–Ga solution.

In this work we propose a multi-scale and multi-physics approach to develop a better understanding of heat transfer and oxygen diffusion in urania (UO_2), a widely used nuclear fuel material. The method requires a theoretical framework to allow for prediction of phenomena such as phase stability, heat transfer, species diffusion, and fission products retention. As a first step, several methods are used at specific time and length scales to determine properties of UO_2.

Fig. 1 shows the time and length scales that are involved in the simulations and the main theoretical methods that are currently used at Los Alamos National Laboratory to develop the models. The multi-scale method relies on enhanced contributions from the electronic structure theory and atomistic calculations. Electronic structure calculations are used to derive the parameters of the inter-atomic potentials. The potentials are validated against a minimal set of thermo-mechanical data. The use of molecular dynamics allows for incorporating vibrational components of thermodynamic properties. Using atomistic methods, the free energy of point defects is determined and the concentration of various types of defects calculated. That serves as input for developing models of non-stoichiometry, thermal conductivity, and oxygen diffusivity. This information is then provided to continuum level simulations of transport phenomena such as

* Corresponding author. Tel.: +1 505 667 8726; fax: +1 505 667 8021.
E-mail address: mastan@lanl.gov (M. Stan).

0925-8388/$ – see front matter © 2007 Elsevier B.V. All rights reserved.
doi:10.1016/j.jallcom.2007.01.102

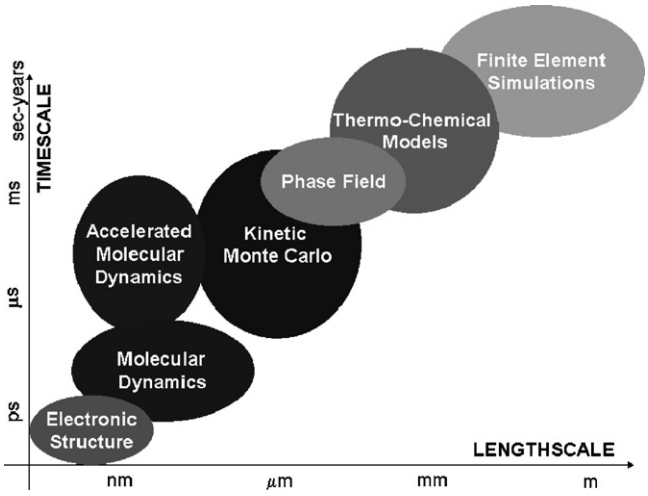

Fig. 1. Length and time scales involved in simulating phenomena relevant for nuclear materials as covered by computational methods.

heat conduction and oxygen diffusion. In this method, the information is transfer via key material properties such as density, formation and migration free energy, thermal conductivity, and species diffusivity.

At this time we are not able to fully interconnect the components and more work is necessary before producing reliable simulations. In this paper, we present preliminary steps towards integrating various length and times scales into a self-consistent simulation of transport phenomena in a nuclear fuel element. To reach the level of precision required by the multi-scale method, the properties are determined with high accuracy. However, the link between scales is imperfect and sometimes missing. Future studies will be dedicated to improving the transfer of information and determining the uncertainty associated with the models and simulations.

2. Results and discussion

2.1. Finite element simulations of heat transport and species diffusion

The temperature and oxygen distribution in UO_2 nuclear fuels are influenced by several phenomena such as neutron flux gradients that produce non-uniform fission density, volumetric heat rate and fission product yields, density changes including swelling, radial cracks, and porosity formation, and microstructural changes such as recrystallization and grain growth. In this work we are focusing on the coupled heat transport and oxygen diffusion phenomena, as a first step towards a more complex study. In a typical fuel element, cylindrical UO_2 fuel pellets are stacked in a metal alloy cladding and the gap between the cladding and the fuel pellet is filled with helium. The fission reaction generates heat that is diffused mostly outwards in the radial direction. Due to the Soret effect, the gradients in temperature induce oxygen diffusion which in turn triggers the conventional Fickian diffusion. The counterbalancing effects of the Soret and Fickian fluxes are responsible for a variation of

Table 1
Summary of materials properties (temperature in K)

Property	Dependence on temperature $T(K)$ and stoichiometry x		Units	Source
$F(UO_2)$	$F(T,x) = \dfrac{2+x}{2(1-3x)(1-2x)}$			[5]
$Q^*(UO_2)$	$Q^*(x) = -1380.8 - 134435.5\exp(-x/0.0261)$		J mol^{-1}	[6]
$\rho\ (UO_2)$	$10960(a+bT+cT^2+dT^3)^{-3}$,	$a = 0.997, b = 9.082\times10^{-6}$ $c = -2.705\times10^{-10}, d = 4.391\times10^{-13}$ } $T < 923$ K, $a = 0.997, b = 1.179\times10^{-5}$ $c = -2.429\times10^{-9}, d = 1.219\times10^{-12}$ } $T > 923$ K	kg m^{-3}	[6]
$k(UO_2)$	$k(T,x) = \lambda0(T)\dfrac{\arctan[\theta(T,x)]}{\theta(T,x)} + 5.95\times10^{-11}T^3$ $\lambda0(T) = [3.24\times10^{-2} + 2.51\times10^{-4}T]^{-1}$ $\theta(T,x) = 3.67\exp(-4.73\times10^{-4}T)\sqrt{2x\lambda0(T)}$		W m^{-1} K^{-1}	[7]

oxygen concentration through the fuel pellet even at steady state [3,4]. Conversely, the temperature variation through the pellet is preserved because of the heat generation, which manifests itself as a source term in the heat equation. The oxygen diffusion equation contains two driving forces: a Fickian term, ∇x, and a Soret term, $xQ^* \nabla T/(FRT^2)$, where T is temperature, R the gas constant, F the thermodynamic factor [5] and Q^* is the heat of transport of oxygen [6]. Table 1 summarizes the expressions used in the simulation, including the density ρ [6] and thermal conductivity k [7] of the fuel.

We used a finite element model to examine the case of fully radial heat conduction and oxygen diffusion, at steady state. The temperature distribution was calculated in the fuel, gap and cladding while the non-stoichiometry was only calculated in the fuel. We use typical radius values of $R_{rod} = 4.3$ mm and $R_{clad} = 4.833$ mm, and a gap of 0.03 mm, although it is known that the gap can vary during the first irradiation cycle. For the temperature in the outer face of the metal alloy cladding, we set Dirichlet boundary conditions by fixing the temperature at 750 K. Similarly, for the outer edge of the fuel rod, the non-stoichiometry was set to 0.001. This value describes a quasi-stoichiometric oxide in equilibrium with the inert gas in the gap. For the heat generation rate due to the fission reaction, we used a typical value of $Q = 4.304 \times 10^8$ W m^{-3} [8].

The temperature and non-stoichiometry distributions along the radial direction of a fuel rod were calculated and are shown in Fig. 2 with solid and dashed lines, respectively. The heat generation due to the fission reaction caused the temperature within the rod to be the highest at the center. Since heat is extracted from the outer surface of the cladding, the temperature decreased with increasing radius, as expected. The oxygen atoms re-distributed such that hyperstoichiometry was higher in the hotter regions. The results are consistent with known behavior of UO_2 fuels and represent solutions of a 1D problem. However, it was important to numerically solve the coupled heat and mass transport equations to gain confidence in the computational tool for further studies of coupled 3D phenomena in UO_2 fuel elements.

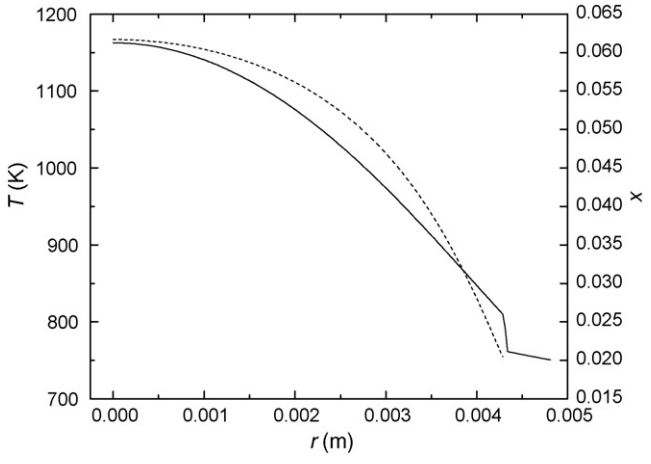

Fig. 2. Steady-state temperature (solid) and non-stoichiometry (dashed) distribution in radial direction for a UO_{2+x} fuel rod.

2.2. Thermochemical models of defects and calculations of oxygen diffusivity

Understanding the structure and the properties of defect lattices is of fundamental importance in materials science, since the atomistic mechanisms control the bulk transport phenomena. Most of the critical parameters influencing the behavior of a nuclear fuel rod, such as species diffusivity and thermal diffusivity, depend on both fuel local stoichiometry and temperature distribution. In particular, multi-scale modeling of the kinetics of oxygen diffusion in non-stoichiometric oxides is a critical component of the combined experimental and theoretical effort aimed at predicting the long time properties and phenomena in nuclear fuel materials. Advancing the thermochemistry of defect species opens a path to modeling of more complex phenomena, such as fission products diffusion [9].

Although UO_2 oxide adopts the same fluorite structure as CeO_2 and PuO_2, the process of reduction of U^{4+} to U^{3+} requires significantly more energy, with the result that in urania the hypostoichiometry can only be measurable at very high temperatures (above 1800 K) and very low partial pressures of oxygen. In UO_{2+x}, a facile valence change U^{4+} to U^{5+} replaces the reduction of metal ions, a mechanism that leads to a wide range of hyperstoichiometry, up to at least $UO_{2.3}$. Such a different behavior from other similar oxides, such as CeO_2 and PuO_2, indicates that not solely the lattice symmetry is involved in the details of evolution toward thermodynamic equilibrium with a given surrounding oxygen atmosphere. The nature, the strength, and the fine details of complex interactions of constituent atoms also play an important role. As first shown by neutron diffraction studies [10], the excess oxygen ions are incorporated at interstitial sites.

The concentration of oxygen atoms is often expressed in terms of the non-stoichiometry x in UO_{2+x}, which is strongly related to the type and concentration of point defects. To calculate the non-stoichiometry, we analyzed a simple model including four types of point defects as major contributors to the lattice disorder: Frenkel pairs, doubly negatively charged oxygen interstitials O_i'', positively charged $U_U^{\bullet}$ (U^{5+}) uranium ions, and positively doubly charged oxygen vacancies $V_O^{\bullet\bullet}$. In this model, we neglect the release of oxygen due to uranium fission and the complex chemistry associated with that process. To describe the charge state of the system, we used the effective electric charge on the defect, namely the difference between the real charge and that of the species that would have occupied that site in a perfect crystal. The cation (U) sublattice was treated as ideal, in the sense that the concentration of uranium vacancies V_U and uranium U_i interstitials were both considered negligible. The model assumed the dilute solution approximation, neglecting at this stage the defect interactions and the spatial correlations due to the exclusion effects. The defect species equilibrium was consequently described using the mass action equations, supplemented by charge conservation and lattice geometry constraints. This statistical thermodynamic approach was incorporated in a Mathcad simulation program. Using as input parameters the enthalpies and the entropies associated to the equations describing the formation of defect species

Table 2
The optimized enthalpy (h), and entropy (s) parameters associated with the defect reactions used in the present calculation of defect species concentration in UO_{2+x}

Defect reactions	Optimized parameters	
	h (eV)	s (k_B)
$O_O^{\times} \leftrightarrow O_i'' + V_O^{\bullet\bullet}$	4.52	35
$(1/2)O_2 + 2U_U^{\times} \leftrightarrow O_i'' + 2U_U^{\bullet}$	−0.37	3.32

listed in Table 2, the concentration of defects were determined with the conjugate-gradient method. Consequently, the values were continuously optimized until a self-consistent good agreement with the reported experimental dependencies of x [11] on temperature and partial pressure of oxygen was observed (Fig. 2).

The predicted concentration of defect species in UO_{2+x} is shown in Fig. 3(a). The Frenkel pairs are seen to dominate the stoichiometric region, while the interstitials take over in the deep non-stoichiometric range. A comparison between the target functions and the calculated partial excess Gibbs free energy of oxygen $\Delta G_{O2} = RT \ln P_{O_2}$ as a function of non-stoichiometry x for 1273 K, and 1373 K is shown in Fig. 3(b). The calculated dependence was further used to evaluate the enhancement factor of oxygen diffusivity in UO_{2+x}, as a function of x.

The self-diffusivity, as a function of non-stoichiometry and temperature, was calculated using a semi-empirical dependence:

$$D_s(x, T) = D_0 x \exp\left(\frac{-E_0}{k_B T}\right) \exp(-\theta x) \quad (1)$$

where D_0 (constant) is a diffusivity prefactor, E_0 (constant) related to the effective migration energy, and θ (constant) describes the blocking effect for the migration of interstitials. This form is based on the analysis of the experimental data [12–15] in Fig. 4, and provides a steeper dependence on non-stoichiometry compared to [12]. Here $D_0 = (l^2/6)Z\nu f_c \exp(s_f/k_B T)$, with the jump length $l = (a/4)\sqrt{2}$ and $a \cong 5.4 \times 10^{-10}$ m the lattice constant, $Z = 12$ is the geometric factor of frequency, $f_c = 2/3$ is the correlation factor, $s_f = 3.32\, k_B$ is the formation entropy of interstitials (see Table 2) and $\nu = 0.996 \times 10^{12}\ s^{-1}$ (in house atomistic calculations). E_0

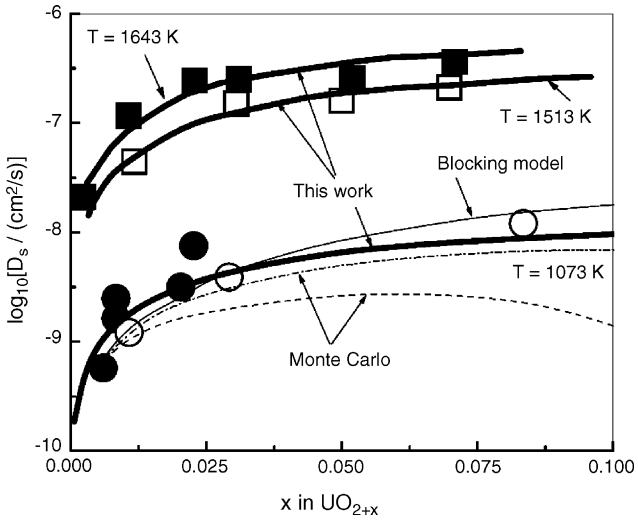

Fig. 4. Oxygen self-diffusion data for UO_{2+x} as a function of composition. Black circles: [12]. Open circles: [13]. Dash dot and dash line: Monte Carlo at $T = 1073$ K [14]. Black squares and open squares: compilation using a collection of experimental data presented in [15]. Thin line: blocking model: [12]. Thick line: this work, calculated with Eq. (1) and $D_0 = 0.013\ cm^2\ s^{-1}$, $E_0 = 1.039$ eV, $\theta = 6.1$.

and θ were derived using Eq. (1) and the available experimental data. The model based on Eq. (1) predicts the appearance of a maximum:

$$D_{s,m} = \left(\frac{D_0}{\theta}\right) \exp\left[-\left(\frac{E_0}{k_B T}\right) - 1\right] \quad (2)$$

in the dependence of self-diffusivity, at a non-stoichiometry x_m satisfying $x_m \theta = 1$. The reasons for the occurrence of a statistically significant maximum around $x = 0.1$ were also discussed by Murch [14]. Recently, preliminary investigations of UO_{2+x} using a simple, but powerful, diffusion simulation of oxygen in UO_{2+x}, based on kinetic Monte Carlo (kMC) procedure [16], predicted oxygen self-diffusivities having the same form and magnitude as given by Eq. (1). The chemical diffusivity was calculated by dividing the self-diffusivity with the correlation factor, and multiplying with the enhancement factor (also called thermodynamic factor).

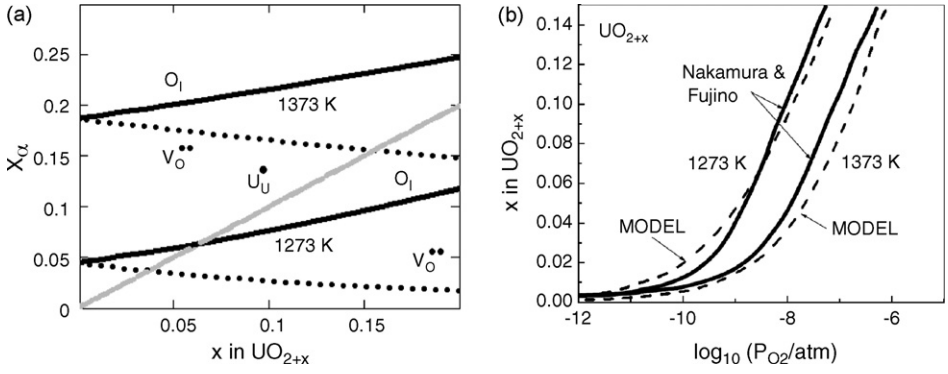

Fig. 3. (a) Concentrations of defect species in UO_{2+x} relative to the concentration of oxygen sites in the perfect lattice, as a function of non-stoichiometry, calculated with the defect model. (b) UO_{2+x} non-stoichiometry as a function of partial pressure of oxygen. Thick line: target functions [11]. Dash line: calculated with the present model.

Fig. 4 shows the calculated self-diffusivity in UO_{2+x} versus non-stoichiometry and temperature. As can be seen, despite simplicity and some rough assumptions, the model predicts diffusivities in a surprisingly close agreement with the experimental results. Since, at this time, the main goal of the model was to relate atomic scale properties of defects to macroscopic oxygen diffusion, we consider this qualitative agreement as satisfactory. We trust that, provided better values of the free energy of formation of different defect types, the agreement with experimental data and the predictive character of the model will improve.

2.3. Phase field simulations of he bubbles formation and evolution

During the last decade, the phase field method has been emerging as a very powerful computational tool for modeling and predicting complex microstructure evolutions on a mesoscopic length scale. It has been applied in many important materials processes [17–21] including solidification, phase separation and precipitation in different alloys, martensitic transformation, ferroelectric and ferromagnetic phase transitions. A phase field model reads thermodynamic and kinetic data from atomistic simulations and thermodynamic calculations, and outputs the kinetic information of microstructure evolution as well as microstructures for calculations on a higher length scale.

In the present work, we developed a phase field model to simulate the evolution of gas bubbles in a single crystal with gas atoms. We assumed that the gas bubble and solution phases are in equilibrium at a temperature of interest. In the phase field framework, a composition field $c(r, t)$ is employed to describe the mole fraction of gas atoms, where r and t are the spatial coordinate and time, respectively. The total free energy of the system, which includes chemical free energy, interfacial energy, and elastic energy, is given as

$$F(c(r,t)) = \int_V \left[G(c(r,t)) + \frac{\kappa^2}{2}|\nabla c(r,t)|^2 + E^{\text{elas}}(c(r,t)) \right] \mathrm{d}V \tag{3}$$

where $G(c(r, t)) = G_0[2.1(c(r, t) - 0.5)^4 - (c(r, t) - 0.5)^2]$ is a double well chemical potential. It has equilibrium values 0.988 and 0.012 for the gas bubble and solution phases, respectively. G_0 is a constant. κ is a gradient coefficient associated with the interfacial energy, and $E^{\text{elas}}(c(r, t))$ is the elastic energy due to the size mismatch between the host and gas atoms. We assumed that the gas bubble is compressible, but cannot resist the shear deformation. The elastic constants are simply written as $\lambda_{ij} = \lambda^0_{ij} + \lambda'_{ij}c(r, t)$ which let the shear modulus in gas bubbles be zero. The elastic energy is calculated by solving the mechanical equilibrium equations in an elastically inhomogeneous solid with an iteration method [18]. The bubble evolution or the gas atom diffusion is described by the Cahn–Hilliard equation:

$$\frac{\partial c}{\partial t} = \nabla M \nabla \frac{\delta F(c(r,t))}{\delta c(r,t)} + \xi(r,t) \tag{4}$$

where M is related to the mobility of the gas atom, and $\xi(r, t)$ is the thermal fluctuation term. In the simulations, we considered a two-dimensional problem although the model is general in three dimensions. Periodic boundary conditions are applied to a simulation cell $256\Delta x \times 256\Delta y$ in the x- and y-directions. The model parameters are listed in Table 3. The kinetic Eq. (4) is solved numerically using a Fourier-spectral method [22]. We assumed that the gas atom has very low solubility in the matrix, and the thermal fluctuation is able to nucleate the gas bubbles. Fig. 5 shows the whole process of gas bubble evolution from homogeneous nucleation, growth to coalescence. The shades of gray denote the concentration of gas atoms. Comparing the gas bubble evolution with and without the elastic interaction, we found that the elastic interaction speeds up the growth of gas bubbles, but slows down the coalescence. More detailed results will be presented in a future paper.

Table 3
Phase field model and simulation parameters

Grad size	$\Delta x = \Delta y = 2.5$ nm
Interface thickness	$\kappa = 1.2 \times 10^{-4}\sqrt{J/m}$
Mobility	$M = 1.5 \times 10^{-28}$ m^5/Js
Elastic constants	$\lambda^0_{11} = 300$ GPa; $\lambda^0_{12} = 100$ GPa; $\lambda^0_{44} = 100$ GPa; $\lambda'_{11} = -100$ GPa; $\lambda'_{12} = 100$ GPa; $\lambda'_{44} = -100$ GPa
Overall composition	$c_0 = 0.23$
Coefficient	$G_0 = 3.6 \times 10^{10}$ J/m^3

2.4. Kinetic Monte Carlo simulations of radiation damage

Kinetic properties of point defects govern radiation tolerance, fission product accommodation, fission gas release and microstructural evolution in-pile [23]. The kinetics of this evolution will impact the stability of the fuel during service. Modeling the defects and the mobility of oxygen in oxide fuels opens a path to the modeling of the more complex phenomena of fission products diffusion. Under operating conditions, urania fuel is typically hyperstoichiometric, i.e., there are excess oxygen atoms in the materials to accommodate U^{5+} charged ions. In hyperstoichiometric UO_{2+x}, the excess oxygen atoms occupy interstitial sites. The thermal conductivity and oxygen diffusivity are inter-related. Under operating conditions, the oxygen atoms re-distribute in accordance with temperature gradients and also serve as carriers for the heat conduction in the urania fuel rod. Thus, understanding oxygen interstitial diffusion is essential to understanding fuel rod properties both in equilibrium and under operating conditions. While atomistic modeling described in Section 2.1 can be used to calculate defect energetics and defect geometry, microstructural evolution that occurs over long length and time scales are still beyond the reach of such algorithms.

We have developed a kinetic Monte Carlo (kMC) model to study the microstructural evolution due to point defect mobility and their interaction in UO_{2-x}. Interstitials are distributed on octahedral sites on the CaF_2 sublattice, and the oxygen atoms migrate by the interstitialcy mechanism. In this mechanism, the oxygen interstitial displaces an adjacent oxygen atom into a nearby vacant interstitial position on the oxygen sublattice. The rates of migration of the interstitial oxygen atoms and vacancies

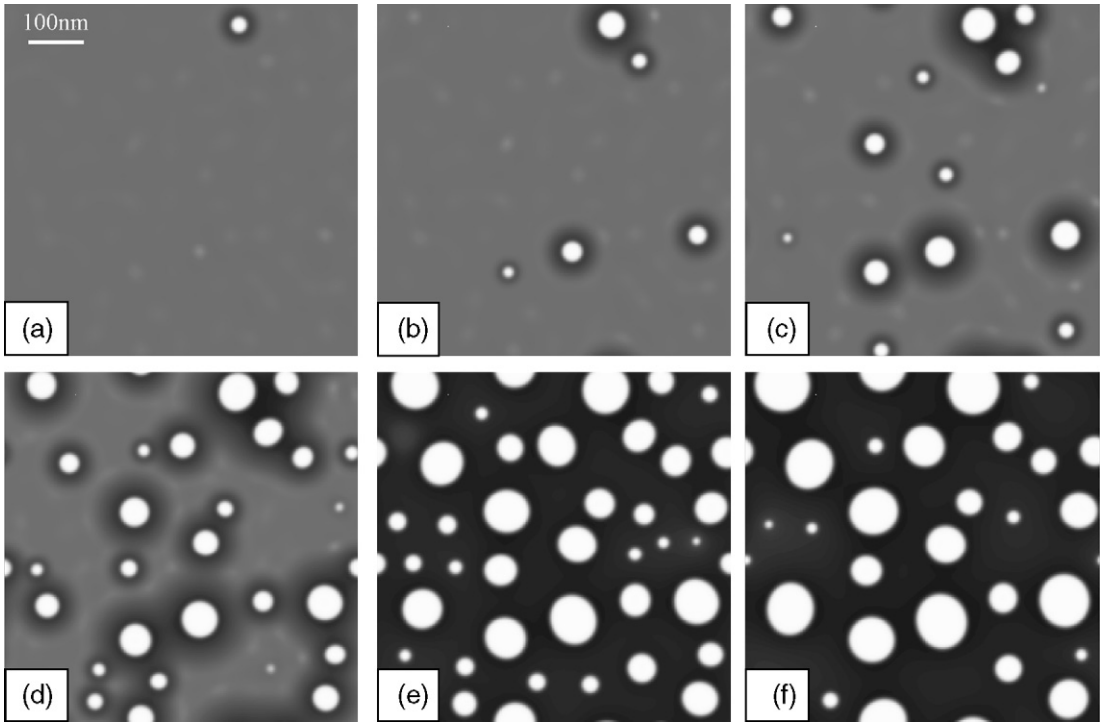

Fig. 5. The temporal evolution of gas bubbles: (a) $t = 10$ s; (b) $t = 50$ s; (c) $t = 100$ s; (d) $t = 150$ s; (e) $t = 250$ s; (f) $t = 350$ s.

on the oxygen sublattice are expected to follow the Arrhenius relation for a thermally activated process: $r = \nu \exp(-E/k_B T)$, where r is the rate, E the activation energy, ν the pre-exponential or attempt frequency factor, T the temperature, and k_B is Boltzmann's constant. Parameters required for the calculation of the rate of migration can be obtained through the atomistic modeling described in Section 2.5. The attempt frequency factor is a constant indicating how many collisions have the correct orientation leading to the transition of the atom from one site to the adjacent site and is taken to be the Debye frequency of UO_2. In the results shown here, the migration rates of the oxygen interstitials and vacancies are calculated by employing activation energies obtained from the experimental deductions by Kim and Olander [24].

A blocking model [25] is employed to describe the interactions between two oxygen interstitials, i.e., if two oxygen atoms are at adjacent interstitial sites, their respective paths in those directions are blocked. The migration of the oxygen interstitials is propagated by the standard kMC algorithm [26,27] in which the simulation time increments are variable and depend on the rates of all the reactions possible in the system.

Using the kMC simulation, we calculate the mean square displacement of the oxygen interstitials. The mean square displacement is related to the diffusivity by the Einstein relation:

$$\mathrm{MSD} = \langle \Delta r^2 \rangle = 6Dt \tag{5}$$

where MSD is the mean square displacement, Δr the displacement of the oxygen interstitial, D the diffusivity and t is the time.

We calculate the diffusivity for different values of the non-stoichiometry for hyperstoichiometric urania. Fig. 6 shows the variation of the oxygen diffusivity as a function of the non-stoichiometry in hyperstoichiometric urania. The diffusivity can be fitted to an expression similar to Eq. (1):

$$D = D_0 x \exp\left(-\frac{E_m}{k_B T}\right) \exp(-\Theta x) \tag{6}$$

where D_0 is the diffusion constant, x the non-stoichiometry, E_m the migration energy of the lattice hop and Θ is the constant describing the exponential dependence on x.

The results of the kMC simulations are compared with data from experimental observations of diffusivity [12,28] in Fig. 6.

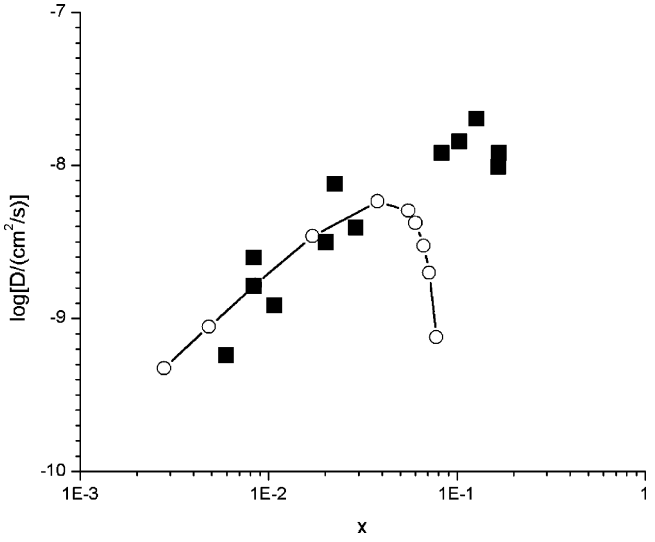

Fig. 6. Oxygen diffusivity as a function of the non-stoichiometry in UO_{2+x}. Circles: Eq. (6), squares: data from [12,28].

At low hyperstoichiometry, the experimental results are closely reproduced by the simulations. The values of diffusivity calculated by the simulations are consistently lower than experimental values at higher hyperstoichiometry.

At low stoichiometry, the diffusivity is dominated by the interstitialcy mechanism which is simulated in the kMC model. Thus the simulations are able to reproduce observed experimental data. At higher stoichiometry, it is possible that the migration of clusters [29] of oxygen interstitials is activated and contributes significantly to the diffusivity of the oxygen interstitials. Such a cluster migration mechanism needs to be accounted for in the kMC simulation which would help explain the large decrease in diffusivity at high stoichiometry. The present result is encouraging because the simulations have been performed with no fitting parameters. Even so, the diffusivities, especially at low stoichiometry, are very close to the experimental results.

Motion of di-interstitial motion is not included in the catalog of rate events. In fact, this is evident in the result where we show lower oxygen diffusivity at higher non-stoichiometry where di-interstitial motion would be more effective. We are presently conducting calculations of the di-interstitial mobility based on ab inito and empirical potentials and will introduce these in the KMC algorithm in order to make the KMC more accurate at higher non-stoichiometric values. So far the values taken in the KMC code are from experimental results. Values of complex mobility based on experimental results are not readily available. We intend to replace our input dataset with a dataset obtained from atomistic calculations.

In the blocking model, oxygen atoms at adjacent interstitial positions repel each other. Thus, Coulomb interactions associated with the excess negative charge of the oxygen interstitials within the UO_2 lattice are considered within the blocking model. Excess charge oxygen atoms are considered purely repulsive. Consequently, di-interstitial complexes are unable to form in the simulation. Once ab initio and semi-empirical calculations of di-interstitial mobility are completed, the KMC simulation will include di-interstitial formation and migration as well. From the results shown in Fig. 6, it is evident that this simple blocking model describes the oxygen transport at low non-stoichiometry. Further changes to the model that reflect di-interstitial formation and migration will make the KMC more accurate at higher non-stoichiometric values.

Future work will refine the kMC model for point defect diffusion in hypo-stoichiometric urania. It is easily possible to incorporate the diffusion of fission products in the kMC model provided the parameters necessary to calculate the migration rates of these products are available. We intend to employ the atomistic simulation techniques (molecular dynamics, density functional theory, accelerated dynamics) to parameterize the input data set necessary for the kMC model to completely describe the mechanisms of oxygen diffusivity as well as fission product mobility in UO_2 fuel rods.

2.5. Atomistic calculations of point defect properties

In this section we calculated defect properties primarily with density functional theory (DFT), to compare both with the simpler empirical potential models and all-electron descriptions of UO_2 described in the next section. The results of these calculations are then used as input into higher-level simulations, such as the kinetic Monte Carlo simulations described earlier.

We have primarily used two different methodologies in this work: density functional theory and accelerated molecular dynamics using an empirical potential.

Density functional theory (DFT) calculations were performed using the VASP [30] code. This code uses pseudopotentials which reduce the core electrons to an effective potential and only explicitly treats the valence electrons. This is in contrast to the calculations of phonon spectra, also reported in this paper, which treat all of the electrons explicitly. We have tested convergence of defect properties versus cell size and k-point sampling, finding that most properties are converged to within 0.1–0.2 eV for a k-point sampling size of $2 \times 2 \times 2$ and a cell size of 24 atoms. This is compared to k-point samplings of $4 \times 4 \times 4$ for the 24 atom cells and cell sizes of 96 atoms. We also verified that our results were insensitive to the spin polarization of the electrons.

The accelerated molecular dynamics simulations employed the temperature accelerated dynamics (TAD) method. This method has been extensively described elsewhere [31]. Here, we note that this method allows for extending the timescale of molecular dynamics simulations to microseconds. We used TAD to probe the kinetics predicted for point defects by a Buckingham model for urania [32]. In our implementation of this model, we did not include the polarizing shells associated with this model. Other results are taken from [33], which did employ the shell model.

Fig. 7 shows the results of calculations for various defect properties in urania. For comparison, we have included the results reported by Crocombette et al. [34] which also employed DFT and those in [33] which are for the Buckingham model mentioned above. All theoretical results are compared to exper-

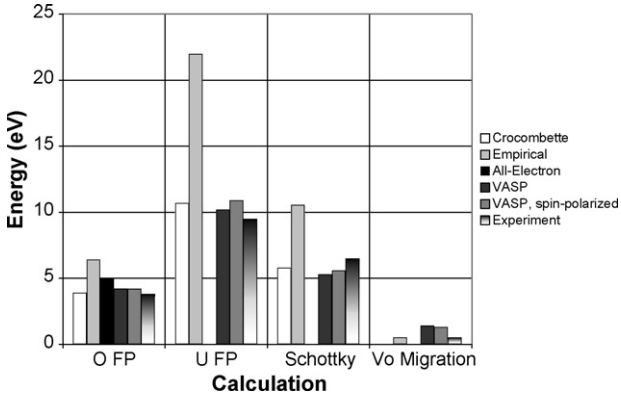

Fig. 7. Defect energies in urania as found via a variety of methods. FP refers to a Frenkel pair defect, while O and U refer to that defect on the oxygen and uranium sublattice, respectively. While electronic structure calculations (VASP and all-electron) tend to agree with experiment for thermodynamic quantities, they do not agree so well for the migration energy of the oxygen vacancy. Rather, the empirical potential, which does not agree well with experiment for defects involving uranium, does agree well with experiment for the migration energy of the oxygen vacancy. Values for experiment and the empirical calculations are from [33] and Crocombette are from [32].

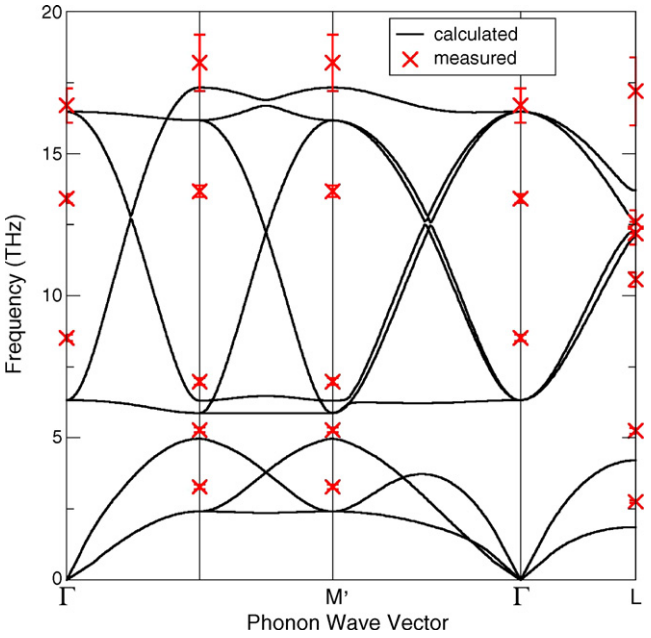

Fig. 8. Measured and calculated phonon dispersion for urania. The measured data is from neutron scattering at 296 K [40], while the calculated frequencies are harmonic and correspond to the low-temperature limit.

imental numbers, as reported in [33] and references therein. As can be seen in Fig. 8, the electronic structure calculations, whether employing pseudopotentials or not, or including spin polarization, all agree well with experiment for all of thermodynamic properties of the defects considered here: the oxygen Frenkel pair formation energy, the uranium Frenkel pair formation energy, and the energy to form a Schottky defect. The empirical potential works reasonably well for the oxygen Frenkel pair, but does not agree with experiment for those defects containing uranium species. In fact, for both the uranium Frenkel pair and the Schottky defect, the empirical potential predicts formation energies that are almost a factor of two greater than experiment. The disagreement for the oxygen Frenkel pair is significantly smaller. There is some sensitivity of the results on the parameterization of the potential, as shown in [33]. These results on formation energies are in contrast, however, with the results for the oxygen vacancy migration energy. In this case, the DFT result is about 1.5 eV, about three times as great as the experimental value of 0.5 eV [35]. The empirical potential actually agrees very well with experiment for this value.

Thus, there is currently no one single theoretical approach that agrees well with experiment for all relevant point defect properties. That the empirical potential does not agree with experiment for all properties is not surprising, since it assumes a fully ionic system which may not be accurate for all aspects of urania. However, the disagreement of the DFT results is a little more surprising until one recognizes that DFT, within both the local density approximation and the generalized gradient approximation, predict urania to be metallic when it should have a gap [34]. This is the standard shortcoming of DFT for band gaps, but illustrates the fact that DFT does not predict all materials properties accurately.

These calculations will ultimately provide input to higher level models such as kMC. Currently, our kMC work uses experimental values for oxygen interstitial migration, which we will replace with atomistic values as we progress in this work. Of key importance is defect–defect interaction, especially interstitial clustering, which will be very important for hyperstoichiometric urania.

2.6. Electronic structure calculations of phonon spectra

Nuclear fuel materials often display properties that make it dangerous to investigate them experimentally. The risk of toxicity or radioactivity leads to precautions that can make the experiments prohibitively expensive. The hazards and expenses limit both number and choice of experiments, which results in insufficient measured data to determine the models needed to investigate potential fuel elements.

Electronic structure methods provide the alternative and step in where experiments become too hazardous or expensive. The scale of what can be calculated is limited to of the order of a 100 atoms, but at that scale modern electronic structure methods deliver reliable input for tuning larger-scale models. In addition, results from these methods can guide the choice of experiments, i.e., the choice of materials worth investigating in the laboratory.

Recent years have seen electronic structure methods used to calculate material properties as they change with temperature—changes that are significant to nuclear fuel materials and their performance. Key to the evaluation of temperature effects is the calculation of individual phonon branches.

As an example, Fig. 8 compares the calculated and measured phonon dispersions for urania. The theoretical frequencies result from applying the direct force method [36–39] to results obtained from density functional theory (DFT) calculations in the generalized gradient approximation. In a large simulation cell consisting of repeated unit cells the force constants are evaluated from the forces on all atoms calculated in response to the displacement of the basis atom in one unit cell. A spatial Fourier transform with a given wave vector q of the force constants results in the q-dependent dynamical matrix. Diagonalization of the dynamical matrix gives the corresponding frequencies. While the frequencies are not in perfect agreement, the overall likeness more than suffices to calculate thermal effects, as these are determined not by the details of individual phonons but by average phonon frequencies.

More importantly, such electronic structure calculations of the phonons deliver reliable tuning of the models described above, especially in terms of how the models describe the influence of temperature on material properties. Thermal effects important to the simulation of nuclear fuels stem from changes in thermodynamics due to changes in chemistry and microstructure; the calculation of these effects quickly becomes prohibitively expensive for electronic structure methods and model potentials must be used.

3. Conclusions

A multi-scale method is proposed for calculating thermo-mechanical properties of nuclear fuel materials and simulating

transport phenomena in nuclear fuel elements. The method consists of electronic structure calculations, development of inter-atomic potentials, molecular dynamics and phase field simulation, and thermo-chemical calculations. The models are incorporated in finite element computer programs and used to simulate the behavior of nuclear fuel materials in reactors. There is a continuous feedback between components, leading to predictions of properties such stoichiometry and oxygen diffusivity, and phenomena such as gas bubble formation and heat transfer. The transfer of information is mediated by properties such as density, free energy, thermal conductivity, and species mobility. At this time, the coupling between methods is imperfect and much work is needed to produce reliable predictions of nuclear fuel behavior in a reactor environment. This work shows preliminary results of such coupling and small steps towards a mechanistic approach that can contribute to the optimization of fuel properties and the evaluation of fuel performance.

Future work will include studies of irradiation effects on thermo-mechanical properties and evaluation of uncertainty. A new method of uncertainty evaluations, based on Bayesian statistics was recently applied to binary systems [41], providing calculated confidence intervals (error bars) for the UO_2–PuO_2 phase boundaries. The method allows for incorporating uncertain data sets, both large and small, in an efficient and meaningful way. Using a similar approach we are currently evaluating the uncertainty of multi-component actinide systems of relevance for nuclear fuels applications.

References

[1] M.I. Baskes, K. Muralidharan, M. Stan, S.M. Valone, F.J. Cherne, JOM 55 (2003) 41.
[2] M.I. Baskes, M. Stan, Metall. Mater. Trans. A 34 (2003) 435.
[3] S.R. De Groot, Thermodynamics of Irreversible Processes, North Holland Publ. Co., Amsterdam, 1951.
[4] C. Sari, G. Schumacher, J. Nucl. Mater. 61 (1976) 192.
[5] T.B. Lindemer, T.M. Besmann, J. Nucl. Mater. 130 (1985) 473.
[6] J.K. Fink, J. Nucl. Mater. 279 (2000) 1.
[7] M. Amaya, T. Kubo, Y. Korei, J. Nucl. Sci. Technol. 33 (1996) 636.
[8] M. Kazimi, et al., Fission gas release models of heterogeneous fuels for plutonium burning, in: Presentation at the Proceedings of MIT Center for Advanced Nuclear Energy Systems.
[9] M. Stan, P. Cristea, J. Nucl. Mater. 344 (2005) 213.
[10] B.T.M. Willis, Solid State Commun. 2 (1964) 23.
[11] A. Nakamura, T. Fujino, J. Nucl. Mater. 167 (1989) 36.
[12] P. Contamin, J.J. Bacmann, et al., J. Nucl. Mater. 42 (1972) 54.
[13] G.E. Murch, D.H. Bradhurst, H.J. de Bruin, Phil. Mag. 32 (1975) 1141.
[14] G.E. Murch, Diff. Defect Data 32 (1983) 9.
[15] J. Belle, J. Nucl. Mater. 30 (1969) 3.
[16] B.P. Uberuaga, M. Stan, C. Deo, P. Cristea, S.G. Srivilliputhur, S. Rudin, J. Wills, T. Patten, Proceedings of the Materials Science and Engineering for Nuclear Fuels Workshop, Los Alamos, NM, USA, 2005.
[17] A. Karma, Phys. Rev. Lett. 87 (2001) 115701.
[18] S.Y. Hu, L.Q. Chen, Acta Mater. 49 (2001) 1879.
[19] Y.L. Li, S.Y. Hu, Z.K. Liu, L.Q. Chen, Appl. Phys. Lett. 78 (2001) 3878.
[20] Y. Wang, A.G. Khachaturyan, Acta Mater. 49 (2001) 2309.
[21] J.W. Cahn, Acta Metall. 9 (1961) 795.
[22] L.Q. Chen, J. Shen, Comput. Phys. Commun. 108 (1998) 147.
[23] M. Stan, P. Cristea, Trans. Am. Nucl. Soc. 91 (2004) 491.
[24] K.C. Kim, D.R. Olander, J. Nucl. Mater. 102 (1981) 192.
[25] G.E. Murch, Phil. Mag. (1975) 1129.
[26] A.B. Bortz, M.H. Kalos, et al., J. Comp. Phys. 17 (1975) 10.
[27] K.A. Fichthorn, W.H. Weinberg, J. Chem. Phys. 95 (1991) 1090.
[28] J.F. Marin, P. Contamin, J. Nucl. Mater. 30 (1969) 16.
[29] B.T.M. Willis, Proc. Roy. Soc. London, Ser A 274 (1963) 122.
[30] G. Kresse, J. Hafner, Phys. Rev. B 47 (1993) 558;
G. Kresse, J. Hafner, Phys. Rev. B 49 (1994) 14251;
G. Kresse, J. Hafner, Phys. Rev. B 55 (1996) 11169.
[31] A.F. Voter, F. Montalenti, T.C. Germann, Ann. Rev. Mater. Res. 32 (2002) 321.
[32] G. Busker, A. Chroneos, R.W. Grimes, J. Am. Ceram. Soc. 82 (1999) 1553.
[33] M. Abramowski, PhD Thesis, Imperial College, 2001.
[34] J.P. Crocombette, F. Jollet, L. Thien Nga, T. Petit, Phys. Rev. B 64 (2001) 104107.
[35] H. Matzke, J. Chem. Soc., Faraday Trans. 2 (83) (1987) 1157.
[36] K. Kunc, R.M. Martin, Phys. Rev. Lett. 48 (1982) 406.
[37] S. Wei, M.Y. Chou, Phys. Rev. Lett. 69 (1992) 2799.
[38] W. Frank, C. Elsasser, M. Fahnle, Phys. Rev. Lett. 74 (1995) 1791.
[39] K. Parlinski, Z-.Q. Li, Y. Kawazoe, Phys. Rev. Lett. 78 (1997) 4063.
[40] G. Dolling, R.A. Cowley, A.D.B. Woods, Can. J. Phys. 43 (1965) 1397.
[41] M. Stan, B. Reardon, CALPHAD 27 (2003) 319.